



HAL
open science

Crustal and upper mantle structure beneath the Corinth rift (Greece) from a teleseismic tomography study

Christel Tiberi, Hélène Lyon-Caen, Denis Hatzfeld, Ulrich Achauer, E. Karagianni, A. Kiratzi, E. Louvari, D. Panagiotopoulos, I. Kassaras, G. Kaviris, et al.

► To cite this version:

Christel Tiberi, Hélène Lyon-Caen, Denis Hatzfeld, Ulrich Achauer, E. Karagianni, et al.. Crustal and upper mantle structure beneath the Corinth rift (Greece) from a teleseismic tomography study. *Journal of Geophysical Research: Solid Earth*, 2000, 105, pp.28,159-28,171. 10.1029/2000JB900216 . insu-03596929

HAL Id: insu-03596929

<https://insu.hal.science/insu-03596929>

Submitted on 4 Mar 2022

HAL is a multi-disciplinary open access archive for the deposit and dissemination of scientific research documents, whether they are published or not. The documents may come from teaching and research institutions in France or abroad, or from public or private research centers.

L'archive ouverte pluridisciplinaire **HAL**, est destinée au dépôt et à la diffusion de documents scientifiques de niveau recherche, publiés ou non, émanant des établissements d'enseignement et de recherche français ou étrangers, des laboratoires publics ou privés.

Copyright

Crustal and upper mantle structure beneath the Corinth rift (Greece) from a teleseismic tomography study

Christel Tiberi,^{1,2} H el ene Lyon-Caen,³ Denis Hatzfeld,⁴ Ulrich Achauer,⁵ E. Karagianni,⁶ A. Kiratzi,⁶ E. Louvari,⁶ D. Panagiotopoulos,⁶ I. Kassaras,⁷ G. Kaviris,⁷ K. Makropoulos,⁷ and P. Papadimitriou⁷

Abstract. We report here the results of a tomographic lithospheric study in the area of the Corinth and Evvia rifts (Greece), designed to constrain the mechanism of continental extension. Sixty seismological stations were deployed in the area for a period of 6 months, and 177 teleseismic events were recorded by more than five stations and gave more than 2000 travel time residuals (*P* and *PKP* phases), which were inverted to image the velocity structure down to 200 km depth. We use both a linear and a nonlinear method to invert the data set. The main result is a long-wavelength positive velocity anomaly located in the upper mantle, which is interpreted as the subducted African lithosphere. The subducted lithosphere is well defined from ~ 70 km depth down to 200 km. From synthetic tests as well as from the amplitude of the anomaly (more than +7%) we conclude that the subduction continues below 200 km. In addition, a second positive velocity anomaly of about +4% from the surface down to 40 km depth, located north of the Gulf of Corinth, has been found. This is interpreted as the result of a crustal thinning of several kilometers (~ 5 km), shifted to the north from the Gulf of Corinth and trending obliquely NW-SE. We suggest that this crustal thinning is mainly related to the Miocene widespread extension in the Aegean and that the Quaternary Corinth rift initiated where the crust was already thinned. The different styles of deformation of the eastern and western part of the rift are consistent with this interpretation. No clear velocity anomaly can be related to the Evvia rift.

1. Introduction

It has long been recognized that the Aegean is one of the most active continental extensional regions in the world [e.g., *McKenzie*, 1978a; *Le Pichon and Angelier*, 1979; *Roberts and Jackson*, 1991]. Owing to its relative small dimensions and to the accessibility of the extensional structures, numerous geophysical and geological observables are avail-

able in this area. It is thus a key place to study the processes involved in continental extension.

The Aegean is located in the western part of the Mediterranean region (Figure 1), where the African lithosphere converges toward Eurasia with a rate of ~ 1 cm yr⁻¹ or less [*Argus et al.*, 1989; *Noomen et al.*, 1996; *McClusky et al.*, 2000]. This convergence takes place along the Hellenic arc [*Taymaz et al.*, 1990], where the African slab subducts beneath the Aegean with a relative motion of ~ 3.5 cm yr⁻¹. This rate is due partly to the African-Eurasia convergence motion (≤ 1 cm yr⁻¹) and partly to the extension of the whole Aegean region (~ 3 cm yr⁻¹). This particular scheme is probably the reason for the unusual shape of the subducted African lithosphere: It is almost horizontal beneath the Peloponnissos and steepens rapidly beneath the Gulf of Corinth [*Hatzfeld et al.*, 1989; *Papazachos et al.*, 2000].

The continental extension in the Aegean region was initiated in Miocene time, probably by the gravitational collapse of the Hellenides mountains [e.g., *Le Pichon et al.*, 1995], leading to widespread extension and crustal thinning in the whole Aegean. At present, this extension, which appears to be localized mostly in the northern part of the Aegean, occurs at a rate of ~ 3 cm yr⁻¹ in the SW direction [*McClusky et al.*, 2000]. It is probably preserved by both westward lateral extrusion of the Anatolian block along the North Anato-

¹D epartement de Sismologie, Institut de Physique du Globe de Paris

²Now at  cole et Observatoire des Sciences de la Terre, Universit  Louis Pasteur, Strasbourg, France

³D epartement de G eologie,  cole Normale Sup rieure, Paris

⁴Laboratoire de G ophysique Interne et Tectonophysique, Grenoble, France

⁵ cole et Observatoire des Sciences de la Terre, Universit  Louis Pasteur, Strasbourg, France.

⁶Department of Geophysics, University of Thessaloniki, Thessaloniki, Greece

⁷Department of Geophysics and Geothermy, University of Athens, Athens, Greece

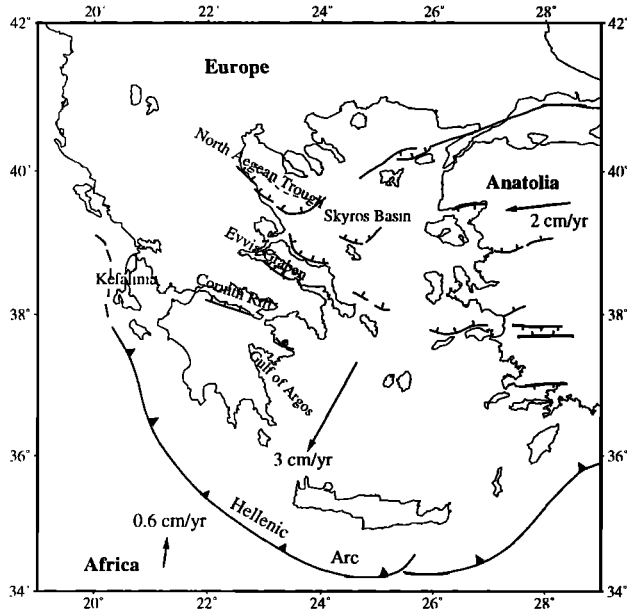


Figure 1. Tectonic framework of the Aegean region. The arrows indicate the direction of movement relative to Eurasia. The velocities are from McClusky *et al.* [2000].

lian Fault (east of Aegean region) and a slab retreat effect of the African lithosphere [Lundgren *et al.*, 1998]. Part of the Aegean extension is now concentrated on land in grabens located at the eastern and western edges of the Aegean region, in Turkey and in Greece [Armijo *et al.*, 1996], as shown on Figure 1. In this paper, we concentrate on two active structures that accommodate part of the Aegean deformation: the Gulf of Corinth and the Gulf of Evvia.

Whereas the central Aegean is now below sea level, the Gulf of Corinth is still an accessible rift edged by clear Quaternary faults, with a high extensional rate ($0.7\text{--}1.5\text{ cm yr}^{-1}$) [Clarke *et al.*, 1997] localized over a width of 10 to 20 km [Briole *et al.*, 2000]. This structure is an asymmetrical half graben, the southern faults being more active than the northern ones (Figure 2). The southern faults show a well-organized en échelon system with Quaternary slip rates that could reach 11 mm yr^{-1} [Armijo *et al.*, 1996]. Although the observational period is not very long, there is some hint that the western and eastern parts of the rift do not deform in the same manner. In the east, fault plane solutions correspond to $45^{\circ}\text{--}50^{\circ}$ dipping normal faults [Jackson *et al.*, 1982; Taymaz *et al.*, 1991], whereas normal faulting mechanisms with shallow ($\leq 30^{\circ}$) north dipping slip planes have been documented in the western part of the rift [Rietbrock *et al.*, 1996; Bernard *et al.*, 1997]. The western part also corresponds to the place where extension is the most rapid and localized. Regarding the Evvia rift, although it is less active than the Corinth rift [Roberts and Jackson, 1991] and presents an extension rate an order of magnitude smaller than that of the Corinth rift [Clarke *et al.*, 1998], it has quite similar tectonic features. Armijo *et al.* [1996] deduced from this similarity a periodic organization of the graben structures along the

edges of the Aegean, which accommodates deformation of the region (Figure 1).

Although a large amount of information is now available for the upper crust in this area, the characteristics and mechanisms of extension at lithospheric scale for these two rifts are poorly constrained. In general, modes of extension are classified into pure shear modes [McKenzie, 1978b], or simple shear modes [Wernicke, 1985]. The pure shear involves a uniform and symmetrical extension in the whole lithosphere, whereas simple shear involves an asymmetrical extension localized along a lithospheric low-angle fault. Some authors [e.g., Lister and Davis, 1989] propose an intermediate mode of extension, where the low-angle normal fault is localized in the upper crust and where pure shear is present in the lower crust. As shown by Allemand and Brun [1991], for example, a symmetrical extension can create asymmetrical structures at the surface. It is thus very difficult to distinguish between pure shear, simple shear, and intermediate mode by simply observing the surficial structures.

Therefore lithospheric structures linked to the Corinth and Evvia rifts need to be better determined in order to shed light on our understanding of the mechanisms of extension in this region. For this purpose, a seismological experiment in the region of the Corinth and Evvia rifts was conducted in 1996. The extension of the array allowed to image the lithosphere down to $\sim 200\text{ km}$.

We present here the results obtained from teleseismic travel time tomography. First, the travel time residuals had been inverted using the Aki, Christofferson, and Husebye (ACH) method [Aki *et al.*, 1977] to obtain the lithospheric structure down to 200 km depth. Second, these results were

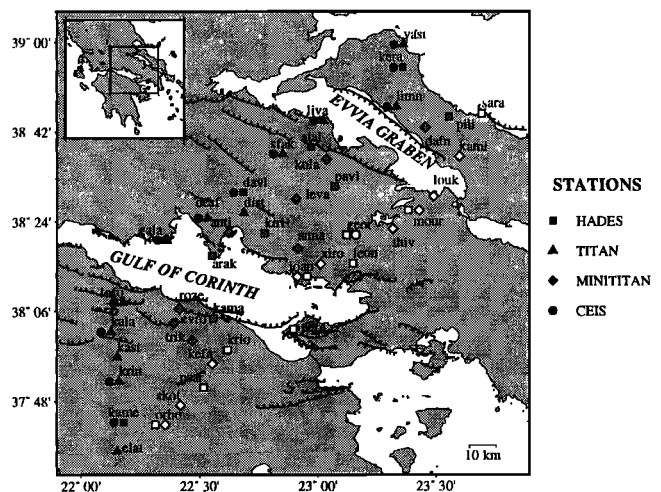


Figure 2. Seismological network deployed during Corinth96 experiment. Each type of station is represented by a different symbol. The array was organized into two main subparallel profiles (east profile in open symbols and west profile in solid symbols). Shaded stations (center of the array) were not used for the residual travel time curves but were used in the inversion. Active normal faults are plotted from Roberts and Jackson [1991], Rigo *et al.* [1996], and Armijo *et al.* [1996].

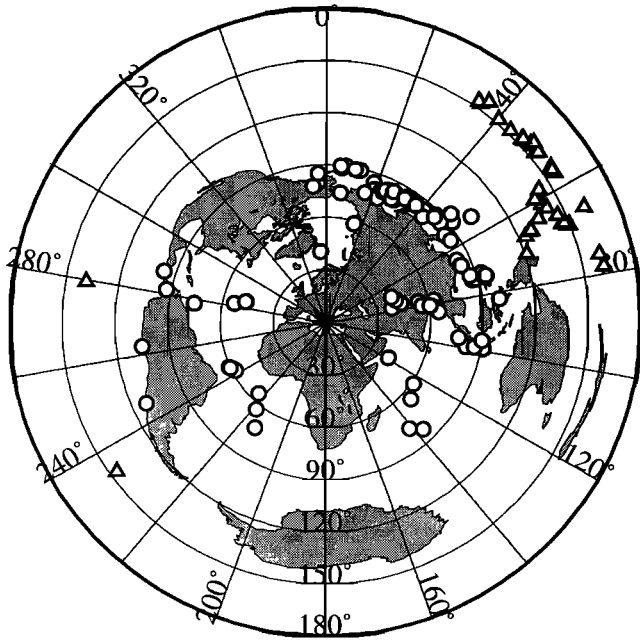


Figure 3. Azimuthal distribution of the 177 events selected in this study in a projection centered on our network. Circles represent *P* wave first arrivals, triangles represent *PKP* wave first arrivals.

compared with those obtained by the nonlinear method of Weiland *et al.* [1995]. In addition, we studied the possibility of artefacts of the inversion due to network geometry, data distribution, and imaged structures, through a series of synthetic tests. Finally, a lithospheric image and a geodynamical interpretation for the Corinth rift that takes into account information from the teleseismic inversion as well as from other seismological and tectonic studies are proposed.

2. Data Analysis

2.1. Experiment

The temporary network deployed from June to December 1996 across the Corinth and Evvia rift system consisted of 60 portable stations installed at 44 different sites (Figure 2). The stations were mainly deployed along two 180-km-long profiles, later on referred to as the eastern and western lines (Figure 2), with an average spacing of ~ 10 km. During the first half of the experiment, an additional 13 stations were deployed covering the area in-between the two profiles. The western profile was equipped with continuous recording stations (Titan) equipped with three-component broadband seismometers (CMG40-20s). The other sites were equipped with event-triggered stations, of the type Hades (equipped with three-component seismometers; Lennartz-5s), Minititan and Ceis (with one-component geophones; 2 s and 1 s, respectively). All stations, except the Ceis, recorded GPS time every hour, allowing for very good control of clock drifts. The internal clock of Ceis stations was controlled by an external Telecode receiver leading in general to a less continuous clock control. Ceis stations were installed in parallel

with Titan stations on the western profile (Figure 2). This allowed us to check the timing precision and to minimize data loss due to enormous power consumption of Titan stations, especially during the winter time. The sampling rate was either 30 (Ceis, Minititan, Hades) or 60 (Titan) samples per second.

We selected 177 teleseismic events that were recorded by more than five stations with epicentral distances $>30^\circ$ and magnitudes >5.0 . The azimuthal distribution of the selected events is shown on Figure 3. The azimuthal distribution is quite good except toward south between 150° and 200° as well as between 300° and 340° . These 177 events yielded 2319 phase pickings, 1748 clear *P* wave first arrivals and 571 *PKP* phases (*PKP_{df}* as well as *PKP_{ab}* and *PKP_{bc}*). *PKP* phases improve the range of near-vertical incidence angles and come mainly from the Pacific region (Vanuatu, Fidji) in our case. After converting all waveforms to a common instrumental response, data were filtered between 0.5 and 5 Hz, and phase pickings were performed using a multi-channel cross-correlation method [Van Decar and Crosson, 1990]. We thus benefit from faster and more accurate processing. Depending on the quality of the phase picking obtained from the cross correlation and on the time correction precision, a time uncertainty was assigned to each residual: 0.03 s for the best ones, 0.05 s for the fair ones, and 0.1 s for the others.

2.2. Travel Time Residuals

Travel time residuals were computed relative to the IASP91 model [Kennett and Engdahl, 1991], using the Preliminary Determination of Epicenters of the U.S. Geological Survey. Then, for each event, relative residuals with respect to the mean of all stations were computed in order to get rid of errors induced by source mislocation, absolute time uncertainty, and differences between the real Earth and standard model outside the target volume. Relative travel time residuals allow us to check the data consistency and to give a first qualitative estimate of the depth, relative sign, and wavelength of the anomalies. Figure 4 presents some examples of travel time residuals curves for different azimuths. Residuals for events with roughly the same azimuth and epicentral distance have been averaged at each station. For each profile the stations were projected on a line passing through the network and trending NE-SW. One can notice that the error bars (associated to phase picking) are always smaller than the global variations of the residuals curve, indicating that the residuals are significant.

The main feature outlined on Figure 4 is a long-wavelength anomaly of up to 1.5 s amplitude, which does not depend much on the profile. Some short-wavelength features are present, probably indicating some weak crustal anomalies, and no particular feature could be clearly associated with the Evvia Graben. The curves are quite similar, with a V shape, and more or less symmetrical. It can thus be expected that long-wavelength velocity anomalies exist perpendicular to the direction of the profiles that do not change a lot between the two profiles. The V shape of the curves indicates a

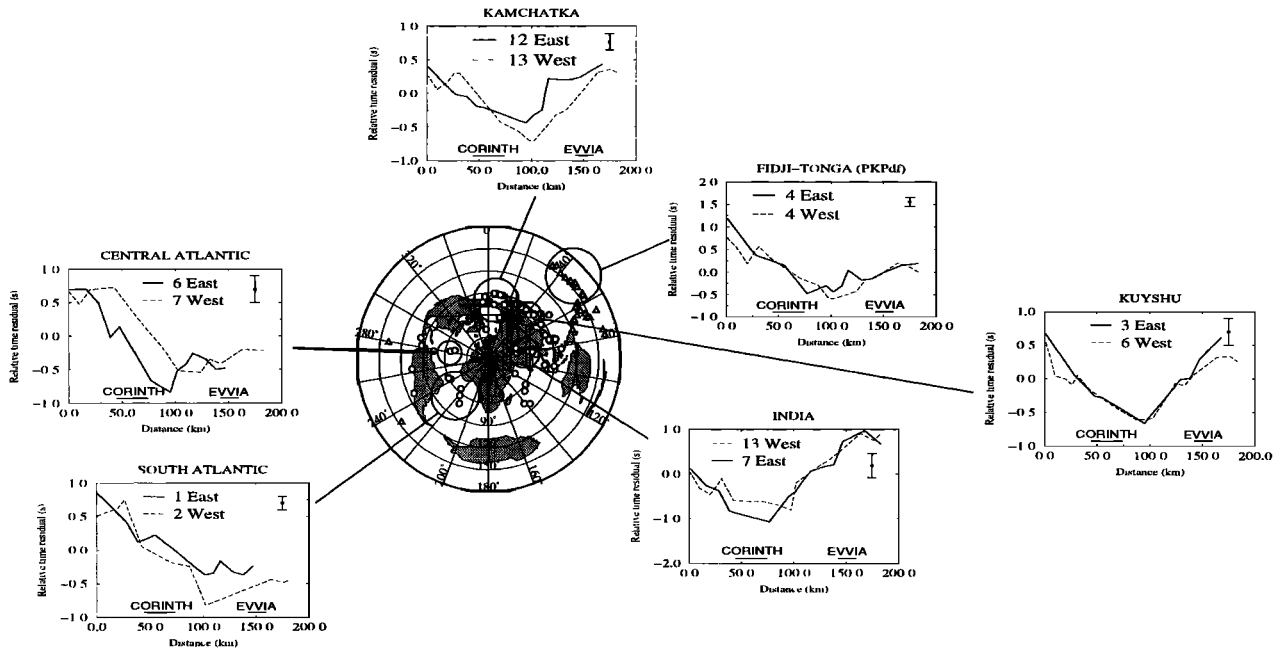


Figure 4. Example of residual travel time curves for various azimuths. The eastern profile is represented as a solid line, the western profile is represented as a dashed line. Error bar in each top corner represents the average scattering of residuals over all the events, obtained from cross correlation. The number of events used for each profile and the location of the Gulf of Corinth and the Evvia Graben are also displayed.

high-velocity anomaly, which probably originates in the upper mantle, as the location of the minimum of the curve depends on the azimuth (for western azimuths the curves lose their V shape to decrease continuously: central and southern Atlantic, Figure 4). The relative peak to peak amplitude of the residuals ranges from 1 s to 1.5 s across 180 km. Such residuals are very likely related to a long-wavelength high-velocity structure in the upper mantle.

3. Inversion

The 2319 phase pickings were inverted for velocity perturbations using the ACH method [Aki *et al.*, 1977], revised by Evans and Achauer [1993]. This method (single step, linear) is particularly suitable for restricted regional networks recording teleseisms. By using teleseismic events we only consider the final part of the ray path, making the assumption that the remaining part of the ray and associated possible errors will be equally affected for all stations. Those error terms can be removed by considering relative residuals. It is thus assumed that the relative residuals express only those heterogeneities located just beneath the array. The inversion is carried out by linearizing the travel time integral into the following matrix expression:

$$\mathbf{G}\mathbf{m} = \mathbf{d}, \quad (1)$$

where \mathbf{G} is the partial derivatives matrix, \mathbf{m} is the vector of the model parameters (unknown velocity perturbations), and \mathbf{d} is the vector containing the travel time residuals. The damped least squares solution of (1) can be written as

$$\mathbf{m}^{\text{est}} = [\mathbf{G}^t\mathbf{W}\mathbf{G} + \theta^2\mathbf{I}]^{-1}\mathbf{G}^t\mathbf{W}\mathbf{d}, \quad (2)$$

where \mathbf{W} is a weighting matrix and θ^2 is the damping parameter. One has to carefully choose the damping factor θ^2 so that there is neither overdamping of the model nor overfitting of the noise. We fixed the value of θ^2 using the empiric trade-off curve between the remaining residual variance after inversion and the squared model length. The optimal θ^2

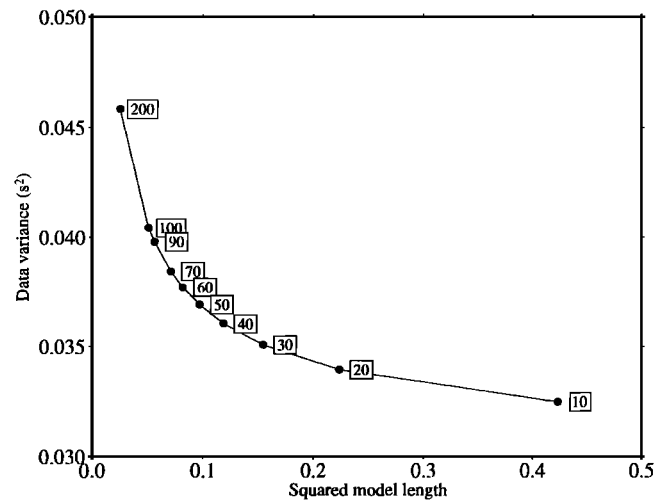


Figure 5. Trade-off curve between data variance after inversion and the squared model length for different damping parameters. A value of 30 s² was selected for this study.

Table 1. Parameters of the Initial 1-D Model for ACH Method

Layer	V_p , km/s ^a	Thickness, km	Blocks 1 ^b	Size 1, km	Blocks 2 ^c	Size 2, km
1 ^d	5.56	10	-	-	-	-
2	6.00	15	8	18	12	22
3	6.50	15	8	18	12	22
4	7.80	25	9	20	18	22
5	8.00	25	10	25	20	25
6	8.15	25	10	30	22	30
7	8.20	25	10	30	22	30
8	8.20	30	10	30	22	30
9	8.50	30	10	30	22	30

^aMean P velocity for the whole layer.

^bNumber of blocks in the main direction of the array.

^cNumber of blocks in the direction perpendicular to the array.

^dSpecial first layer. one cone-shaped cell assigned to each station.

value can be found at the turning point of the curve as the best compromise between overdamping and noise domination. We estimate from Figure 5 that values between 30 and 90 s² seem a reasonable choice. Only small changes in the velocity anomalies amplitude are induced; the location and geometry of the anomalies remain constant. For example, for $\theta^2=30$ and 50 s² a maximum change of $\sim 15\%$ is recorded on the maximum velocity anomalies in poorly resolved areas. We take $\theta^2=30$ s² for this study.

The initial one-dimensional (1-D) model is composed of several homogeneous velocity layers divided into regular blocks. Blocks crossed by < 10 rays were not inverted. The first layer is treated in a special way [Evans and Achauer, 1993]. In this layer, nonoverlapping cones are assigned to each station to account for the fact that rays hardly overlap in the first kilometers. The initial model used in this study is listed in Table 1, while Table 2 displays the main parameters of the inversion. Velocities in Table 1 were chosen from previous studies in the region [Papazachos et al., 1995; Rigo et al., 1996]. The crust is represented by the first three layers of the model, the Moho being at 40 km depth.

We have tested the effect of the initial model by modifying the width, height, and the initial velocity of the layers, as well as the Moho depth. However, none of those changes significantly modified the result. The depth range of the inversion is commonly 2/3 to about the length of the array aperture, depending on the structures and the data [Evans

and Achauer, 1993]. Although the aperture of our array is ~ 180 km, we attempted to invert down to 200 km depth because we expect long-wavelength structures in the upper mantle.

The selected parameters for this study result in a data variance improvement of 85% (Table 2). Results of the inversion are expressed in terms of velocity perturbations relative to a lateral homogeneous model. To avoid block limits artefacts, the offset-average smoothing method as described by Evans and Zucca [1988] was applied. This type of smoothing results in averaging nine inversions, each block parametrization being offset by $\pm 1/3$ in the x and y directions. One should keep in mind that vertical smoothing applied to some vertical cross sections is due to the imaging routine and is not totally correct for the ACH method, as velocity perturbations are relative to a reference velocity for each separate layer (which may change).

4. Results

4.1. Resolution Matrix

Before discussing the results of the inversion and the velocity model obtained by the ACH method, one should check the quality of the inversion by examining the whole resolution matrix which is given by

$$\mathbf{R} = [\mathbf{G}^t \mathbf{W} \mathbf{G} + \theta^2 \mathbf{I}]^{-1} \mathbf{G}^t \mathbf{W} \mathbf{G} \quad (3)$$

with the same notation as in (2). Each diagonal element of this matrix indicates how well the corresponding parameter is resolved. If the resolution was perfect, one would obtain the identity matrix. In our case, nonnull off-diagonal terms as well as negative sidelobes are observed.

The diagonal terms are on average larger than 0.5 with a maximum of 0.81, indicating that the parameters are, in general, well enough resolved to trust the main anomalies of the velocity model. The diagonal terms decrease near the edges of each layer, indicating a better resolution at their center (where there is the best ray cross fire). However, nonnegligible off-diagonal terms are present, and the largest val-

Table 2. Inversion Parameters for the ACH Method

Parameter	Value
Number of blocks	1497
Number of inverted blocks	419
Damping factor, s ²	30
Initial data variance, s ²	0.25
Data variance after inversion, s ²	0.04
Variance improvement, %	85

ues (maximum 0.26, in general, around 0.1) concentrate on lines parallel to the main diagonal and form secondary diagonals. This indicates coupling between neighboring layers. It can be viewed as a vertical smearing effect always present in teleseismic tomography: vertical resolution is inhibited by the subvertical geometry of rays. However, in our case those elements rapidly decrease for the farthest layers (secondary diagonals are larger for the layers immediately above and below). Moreover, the remaining values of off-diagonal elements are small (mostly below 0.03). The diagonal terms of the resolution matrix for each layer are presented in Plate 1 with the corresponding tomograms expressed in terms of P velocity perturbations.

4.2. Crust

The crust has been parametrized with three layers between 0 and 40 km depth (Table 1). The first layer (0-10 km) is not represented because it is not well resolved and corresponds mostly to near-surface and site effects. The resolution panel (Plate 1) indicates that the closer to the center of the layer, the better the blocks are resolved, except beneath the Gulfs of Corinth and Evvia, where low resolution appears in layers 2 and 3 (10-25 km and 25-40 km) owing to the lack of stations in both gulfs.

Velocity perturbations range from -6.2% to +4.8% for layer 2 and from -8% to +3.7% for layer 3, not considering the -12% that appears in only one block of layer 3 (Plate 1) and which is not at all resolved. No clear velocity perturbation is present beneath the Gulf of Evvia. Although the strong negative amplitude localized at the southern part of layer 3 is not very well resolved, it looks consistent with layer 2 and is likely not an artefact of the inversion. The low-velocity zone (-3%) observed on the southern coast of the Gulf of Corinth (near the stations trik and evro, see Figure 2) could be related to the presence of sediments. Indeed, thick layers of Plio-Quaternary sediments are present all along the southern coast of the Gulf of Corinth and could produce the observed anomaly [Armijo et al., 1996; Le Meur et al., 1997].

The main feature that appears in Plate 1 for the crust is the high-velocity contrast of about +4% trending NW-SE being located beneath the northern edge of the Gulf of Corinth. It is 10 to 15 km wide and is present over the whole width of the array. The direction of this anomaly (NW-SE) is neither that of the gulf (N110°) nor the direction of the main presently active normal faults. However, it is more or less the direction of the geological structures (the Hellenides mountains), and it is also orthogonal to the direction of Miocene extension [e.g., Mercier, 1981; Jolivet and Patriat, 1999].

4.3. Upper Mantle

The upper mantle is parametrized by layers 4 to 9 down to 200 km depth (Plate 1). The most striking feature is a high-velocity perturbation trending NW-SE. This perturbation is present from 70 km down to 200 km. Its amplitude varies from about +4% for layer 5 to +7.5% as one goes deeper and is maximal in layer 9 (170-200 km). This high-

velocity region is ~80-90 km wide and seems to dip in the NE direction. This is clearer on the cross section (Plate 2), where it dips with an angle of ~50°. The direction of the section (Plate 2) is the direction of the profiles (NE-SW) and is also roughly the direction of the dip of the African slab in this region [Hatzfeld and Martin, 1992; Papazachos et al., 1995]. Seismicity from the International Seismological Center (ISC) and relocated ISC catalogue [Engdahl et al., 1998] associated with the African slab is also plotted in Plate 2 (only events deeper than 60 km have been plotted). One peculiar observation in this region is that the recorded seismicity stops at a depth of ~200 km, which has led some authors to interpret it as the maximum depth of the slab [e.g., Le Pichon and Angelier, 1979]. However, tomographic studies show that the fast velocity anomaly associated with the slab is continuing below 200 km, maybe as deep as 600 to 800 km [Spakman et al., 1988; Piromallo and Morelli, 1997]. Plate 2 shows a good correlation of the location of the high-velocity anomaly with the location of the hypocenters, even if they seem to concentrate in the lower part of the slab. As the subducting African lithosphere is colder than the upper mantle, it induces a high-velocity anomaly which manifests itself clearly on the cross section.

However, some questions arise from the observation of this fast body on Plate 2: How can one explain the increasing velocity contrast in the deep layers of our model, and why is there apparently no continuity of the slab to the southwest? The deeper part of the slab below 200 km may disturb rays, and those perturbations could be projected into the deeper layers during the inversion, thus accounting for the observed stronger amplitude at depth. From previous studies [Hatzfeld, 1994; Papazachos and Nolet, 1997], we expected to see a near-horizontal part of the slab beneath the Peloponnissos that we do not distinguish in the P wave velocity model, maybe because of the vertical geometry of the teleseismic rays. In addition, one can wonder if the fast crustal velocity anomaly beneath the northern coast of Corinth could be due to a smearing effect of the deeper structures. All these questions will be addressed in section 4.4 with the help of synthetic tests (section 4.5).

4.4. Comparison With Another Method

We performed various synthetic tests in order to better understand the possible artefacts or bias coming from the inversion itself, as well as from the event distribution and the network configuration. Those tests were performed with the inversion scheme of Weiland et al. [1995]. ACH is a linear method using a straight ray approximation, which depends on the size and depth of the anomalies and might not be quite valid. Weiland et al. [1995] proposed a new method using essentially the same inversion algorithm as ACH, but including a 3-D simplex ray tracing [Steck and Prothero, 1991], and iterating the procedure. In order to first test our results obtained by ACH, we performed an inversion on the same data set with the method of Weiland et al. [1995]. The parametrization of this method is quite different from the previous one as it is a 3-D grid of velocity nodes with an

interpolation between each node [Thurber, 1983]. The inversion is performed using a damped least squares method with an a priori constraint on the second derivatives [Menke, 1984]. We proceed the same way as for ACH to determine the damping factor θ^2 and a value of 30 s^2 seemed to be the best choice. To easily compare the results from both methods, the initial 1-D model for this method was similar to that of Table 1, with the depth of each node level fixed to the mid-layer value of the corresponding layer in the ACH model. Seven hundred and fifty nodes were inverted with a spacing of 25 km, and after five iterations the residual variance was improved by 78%.

The locations and sign of the velocity perturbations deduced from this inversion are similar to those from the ACH method for all layers (except the first one, as it is not considered the same way). Hence we will not show the results for all layers but just compare the cross section obtained from this method (Plate 3) with that obtained with ACH (Plate 2). As regards to amplitudes, the method of Weiland *et al.* [1995] results in larger values than ACH. Weiland *et al.* [1995] explain this behavior by the fact that the real amplitudes are better retrieved by an iterative method rather than by a single-step algorithm. All features are identically retrieved, but low anomalies are spread a little more than in the case of ACH. The increase in amplitude for the two deepest layers is much more striking as values as high as +13% are reached at 180-200 km depth (Plate 3).

4.5. Synthetic Test

The increase in amplitude observed in the *P* wave velocity model (Plates 2 and 3) could come from the influence of the remaining part of the slab below 200 km. As the perturbations induced by this structure seem to be symmetrical, a very simple test has been performed. A simple shaped slab running NW-SE with a +5% velocity contrast relative to the background velocity was used as a starting model. The slab is horizontal beneath Peloponnissos as suggested by several authors [e.g., Papazachos and Nolet, 1997], then it dips at 50 to 60°, down to 300 km. At this depth the structure was made larger according to the observations made by Piromallo and Morelli [1997]. Residuals associated with this structure are calculated by removing the travel times through the unperturbed model from the travel times through the model with the +5% velocity structure. Those residuals are inverted using the nonlinear method and the same parameters.

The result of the inversion is displayed in Plate 4, with the synthetic slab delineated by the black lines. The horizontal part of the slab is missing in the output model (Plate 4), confirming the poor vertical resolution due to subvertical rays. A purely horizontal structure can hardly be imaged at depth by teleseismic tomography. Instead, it is smearing all along the path (see the cookbook by Evans and Achauer [1993]). However, for the layers from 70 km down to 200 km, the features are strongly similar to those obtained from the real data (Plate 2): The slab is laterally well imaged, as well as neighboring features. Clearly visible artefacts of low-velocity perturbations appear near the edges of the slab (Plate 4), where

no anomaly had been introduced. These zones can also be observed in Plate 2 and thus should be regarded not as geophysical signal, but rather as artefact. The increasing velocity contrast in the data inversion in the deepest layers is well retrieved in the synthetic test (+13%), showing the effect of the downgoing part of the slab below 200 km depth: In fact, the inversion projects perturbations coming from the lowest part of the slab into the deepest layers of the model, creating these large amplitudes at 200 km depth. Synthetic tests with a slab stopping at 200 km depth did not show an increasing velocity contrast in the deepest layers as observed in our case. Additional tests indicate that the results of the inversion remain unchanged when the horizontal part of the slab is either suppressed or put deeper.

Two others synthetic tests were made in order to understand how the slab structure could interfere with crustal structures and how well the latter could be retrieved. The first test consists in a +10% velocity anomaly located in the layers 1 to 3 of the initial model. The results (Figure 6, left) show that we retrieve a weaker anomaly of +6% in layers 1 to 3, with smearing effects towards layer 4 (+3% velocity perturbation in this layer). Artefacts of opposite sign (-4%) are present on both sides of the initial velocity anomaly. When adding the synthetic slab (Figure 6, right), the structures interfere with each other. The resulting cross section shows quite identical features for layers 4 to 9 as those for the slab alone (Plate 4), but the initial velocity contrast of 10% in the three first layers is enhanced to reach almost +7% in layer 3. The negative artefact in the left part of the cross section is reduced, whereas the one on the right side is enhanced owing to the slab artefact towards the surface.

Therefore it is concluded from these tests that although vertical smearing is present, the anomalies observed in the crust (0-40 km) cannot be explained as artefacts from a deeper slab structure (Plate 4), and that, in addition, surficial structures can be well retrieved even with a subducting slab (Figure 6). In particular, the high-velocity anomaly beneath the northern edge of the Gulf of Corinth and the low velocity beneath Peloponnissos cannot be the effect of the slab. The synthetic tests show that the artefacts created by the slab in the crustal layers are indeed opposite to those observed on Plate 2. These anomalies are thus not artefacts related to a subducted body and should be interpreted as real crustal structures.

5. Discussion

5.1. Subduction

The main part of the final velocity model obtained by inversion is dominated by the influence of the subducted African lithosphere. We obtain a more detailed geometry for this slab from 70 km down to 200 km depth than the previous study of Spakman *et al.* [1988] or Piromallo and Morelli [1997], for example. Nevertheless, the results are in agreement with those studies. In particular, the fact that the dip angle is very small beneath Peloponnissos and increases to a steeper one north of Corinth rift is in common

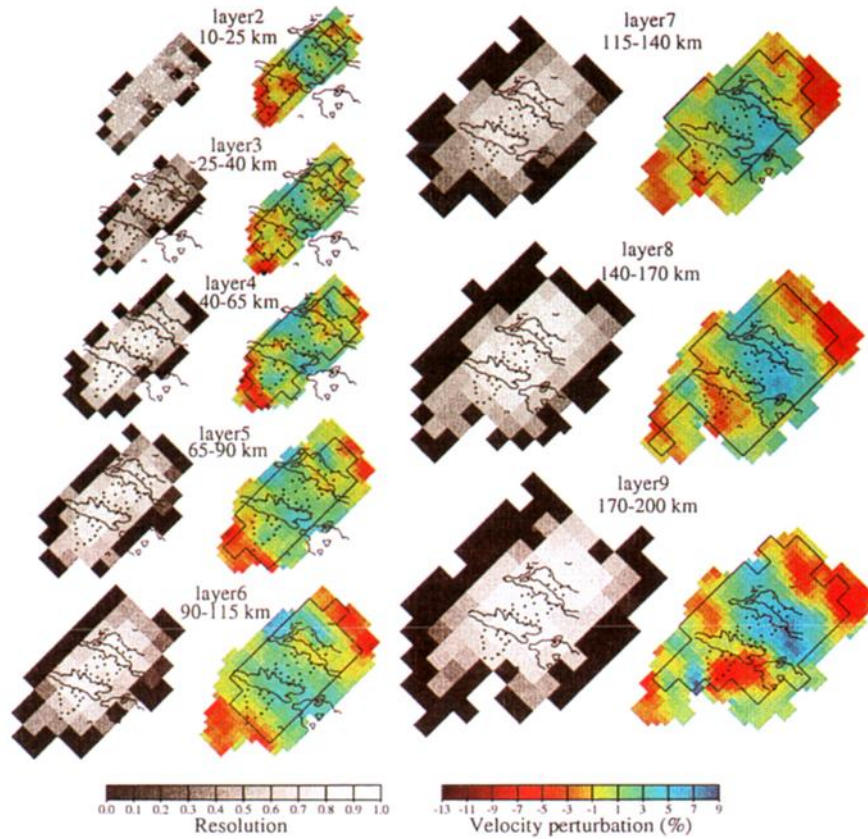


Plate 1. *P* wave velocity perturbations obtained after the ACH inversion and diagonal elements of resolution matrix for layers 2 to 9. The black line on the velocity perturbation pictures represents blocks with a resolution larger than 0.5.

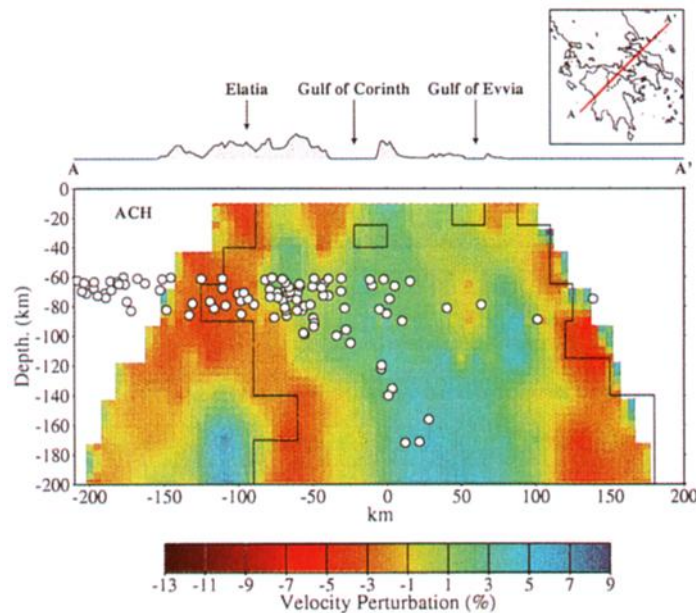


Plate 2. Cross section with *P* velocity perturbation in percent (same color scale as in Plate 1) from ACH. AA' is a SE-NW section along the main direction of the array. Relocated International Seismological Center (ISC) seismicity is reported in white circles [Engdahl *et al.*, 1998].

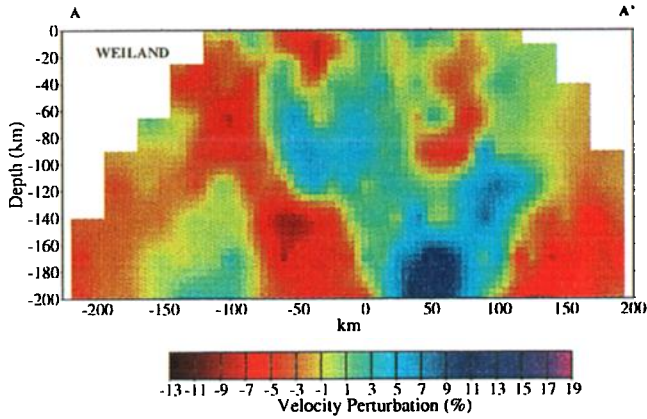


Plate 3. Cross section with P velocity perturbations in percent from *Weiland et al.*'s [1995] method. The color scale is the same as for Plates 1 and 2; it has only been enlarged to fit higher positive values. The section was performed along the same AA' track as for Plate 2.

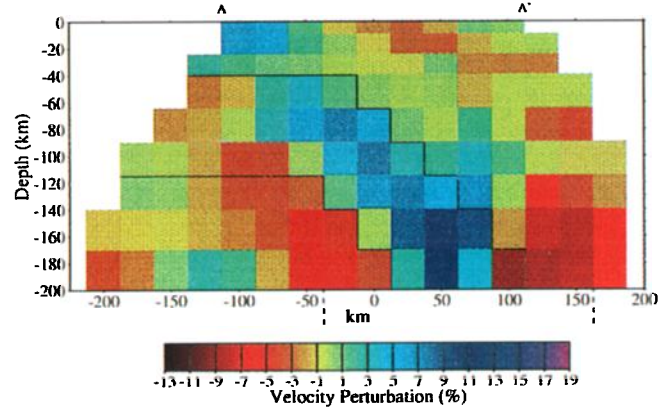


Plate 4. Tomographic cross section along the AA' track obtained from the synthetic model of a slab (P velocity perturbation in percent). The black lines outline the initial high-velocity body (+5%), which continues down to 300 km.

with the study of *Papazachos and Nolet* [1997]. Though the study itself does not give a precise idea of the shape of the slab below 200 km depth, one can argue from the synthetic test presented in section 4.5 that the slab should continue below 200 km depth. This is in agreement with the results of *Spakman et al.* [1988], who follow this structure down to at least 600 km depth. The intermediate seismicity (Plate 1) seems to be concentrated on the lower part of the slab image. However, this can be the effect of two artefacts. The first one comes from the projection of the hypocenter on the cross section. As the slab presents a curved shape along the Hellenic Arc and as the width of projection is 150 km, the seismicity may have been projected lower than it really is. Second, Plate 4 shows that the image of the slab is slightly shifted upward and that the initial limits of the slab are located lower than what the velocity structure suggests. For

these reasons, we think that the intermediate seismicity is most likely located inside the slab structure, rather than at its lower boundary.

The velocity contrast obtained for the African slab is a little higher than that found by *Bijwaard et al.* [1998]. With both methods, *ACH* and *Weiland et al.* [1995], velocity perturbations of about +5% and +7% are obtained for the slab (without considering the lowest layers), whereas *Bijwaard et al.* [1998] report about +3% for the same cross section. In general, subducting slabs show velocity perturbations between +2% and +5%, so taking into account the enhancement of amplitude by the deeper part of the slab (below 200 km), one might explain part of this high amplitude but not all of it. The velocity contrast produced by the African subducted lithosphere could be enhanced by anisotropic effects or waves guided in the slab, resulting in the strong

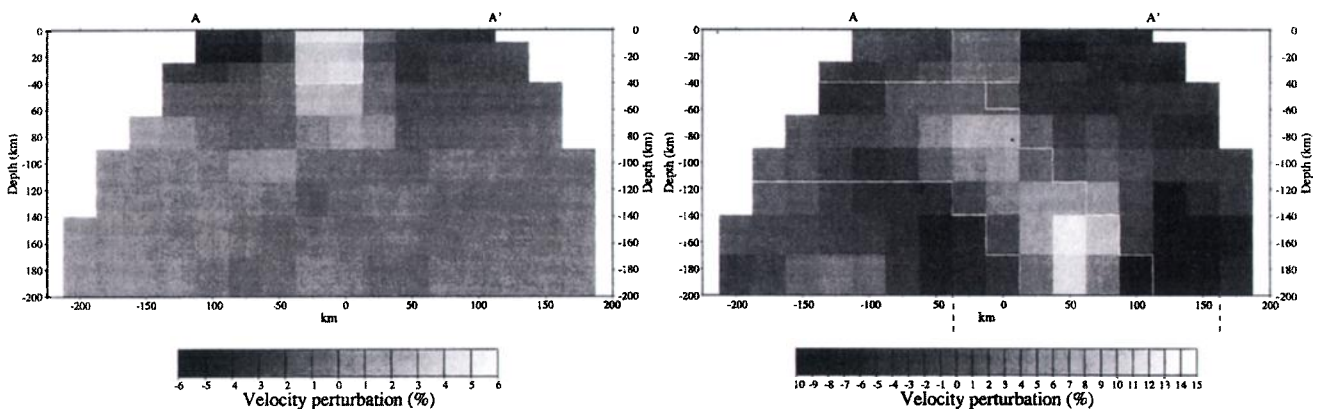


Figure 6. Cross section for synthetic tests with (left) a surface anomaly (+10%) in the three first layers only and (right) a surface anomaly (+10%) with a slab structure (+5%) down to 300 km depth. The limits of the synthetic structures introduced in the model are outlined by white lines.

amplitude observed in our velocity model (more than +6% in Plate 3, for instance). As the main part of the residuals comes from the N-NW azimuth, they correspond to rays coming from the same direction as the dipping plane of the subducted plate, and they could thus be guided in this structure, as proposed by *van der Hilst and Snieder* [1996] for the Kermadec region.

5.2. Gulf of Corinth and Gulf of Evvia

Although the presence of the subducted African lithosphere prevents us from obtaining a well-defined lithospheric structure for the Corinth and Evvia region, we are able to distinguish some important features, especially in the first 40 km. These main features are (1) a low-velocity zone at the southwest extremity of the array and (2) a high-velocity perturbation north of the Gulf of Corinth, in the Beotian area. The synthetic test presented in Plate 4 shows that these anomalies are not due to artefacts but that they are most likely caused by real structures. These structures can be of several origins, and we will discuss three main possibilities: crustal thickening, inherited geological nappe structures, and crustal thinning. It is unlikely that only one of these structures is real and the other a consequence of the ACH method, which tends to average perturbation close to zero within each layer. From synthetic tests we argue that the positive velocity anomaly north of the Gulf of Corinth is not high enough to create -10% of velocity contrast in the SW part of the network. In addition, artefacts coming from negative velocity perturbations in this SW part of the area cannot satisfactorily explain the small lateral extension of the high-velocity anomaly north of Corinth.

5.2.1. Crustal thickening. In this region, the crust is made of a successive stack of nappes of highly heterogeneous materials trending in a general NW-SE direction [*Bonneau*, 1982]. This stack of nappes in the southwestern part of Greece and Peloponnissos resulted in building the Hellenides mountains and in crustal thickening. This is clearly seen in the southwestern part of the region (Peloponnissos), where low-velocity anomalies appear (Plate 1, layers 2 and 3). Although the resolution is poor, it corresponds to the location of a very likely crustal thickening, which should be linked to the presence of the Hellenides mountains. As one goes northeastward (toward the Aegean Sea), the crust is thinning. Consequently, the velocity contrast observed between the low-velocity anomaly in the SW and the fast anomaly located north of the Gulf of Corinth could be explained by this change in crustal thickness. However, this alone cannot be the explanation because of the restricted area of the fast anomaly between Corinth and Evvia. If one only considers the change from a thick crust under Peloponnissos to a thinner crust under the Aegean Sea, the fast velocity anomaly should continue under Evvia and not be limited to a short strip (about 15 km), as in our case (Plate 1).

5.2.2. Inherited geological nappe. To explain the zone of fast crustal velocity north of Corinth, we also examined the hypothesis of the presence of a faster geological nappe with a NW-SE direction. However, none of the struc-

tures reported on geological maps correspond to the well-defined lateral limits obtained by the tomographic inversion [*Mouyiaris et al.*, 1989]. Some ophiolites and metamorphic material can be found at the surface [*Bonneau*, 1982], but they are strongly localized in areas of few square kilometers and are apparently very surficial features. It is unlikely that they will affect the tomograms down to 40-50 km depth. The presence of a large ophiolitic body in this area is also unlikely. The ophiolites are generally organized in lenticular shape zone, unable to produce a +4% velocity anomaly along a 15-km large strip across the whole array. Moreover, some ophiolites are located on Evvia island, and they do not correspond to fast-velocity contrast on the tomograms (Plate 1).

5.2.3. Crustal thinning. The fact that this fast anomaly is consistent with the direction of extension during Miocene suggests a possible cause for this anomaly. The extension could have created a localized crustal thinning where fast upper mantle material could rise. This intrusion of mantle material could provide such a fast-velocity anomaly: a +3% velocity anomaly in the layer 2 and +2% in layer 3, as observed, applied to our initial velocity model could be explained by a mantle upwelling of ~5 km in layer 3. It is obviously not a unique model because in this case, amplitude and thickness of the perturbed layers are linked. However, the next question that rises is whether this crustal thinning can be related to the present location of the rift system (Corinth and Evvia). Indeed, as much as 5 km of crustal thinning seems unrealistic if related to the 1 Myr old extension of Corinth and Evvia rifts alone. In addition, no particular velocity anomaly can be related to the presence of the Evvia Graben, but preexisting structures (Miocene) could explain part of this crustal thinning, as well as the direction of this structure.

As proposed by *Armijo et al.* [1996], during the Miocene, extension could have produced periodic lithospheric instabilities (necking). Those structures could have been created by boudinage [*Martinod and Davy*, 1992]. This boudinage could have produced a primary crustal thinning of few kilometers in the Beotian region, and thus made the initiation of the Corinth rift in this region easier. The rift may have started where the crust was first weakened by these lithospheric instabilities, that is, at the eastern edge of the gulf (Plate 1, layers 2 and 3), where crustal thinning seems to take place. Then, 1 Myr ago, the structures of Corinth and Evvia were reactivated, possibly by the propagation of the North Anatolian Fault [*Armijo et al.*, 1996], but instead of following the direction of the original crustal thinning, the rift is propagating now at the surface in a more westward direction quite rapidly [*Clarke et al.*, 1998], which results in an offset between the crustal thinning and the location of the rift at the surface (Figure 7). Two possibilities could be put forward to explain this offset: preexisting crustal heterogeneities and/or a change in the boundary conditions. In fact, the subduction of the African plate stops north of the Kefalinia Island, and a continental collision occurs, locking the western border of northern Greece (see Figure 1). This is clearly seen on the GPS results from the area [*Kahle et al.*,

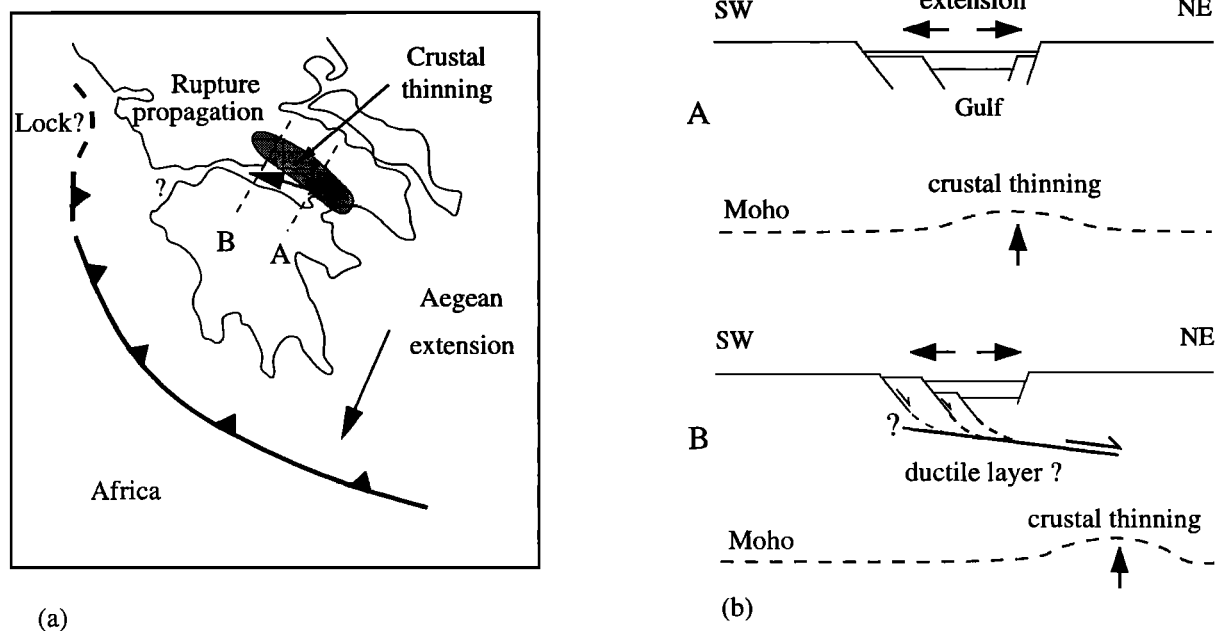


Figure 7. (a) Location of the crustal thinning linked to the Corinth rift structure. This crustal thinning was first created at Miocene time by lithospheric instabilities due to the gravitational collapse of the Hellenides mountains. It could have favored the initiation of the rupture of the Corinth rift, and the propagation of the North Anatolian Fault could have reactivated the extension of the rift. (b) Sketch of crustal structure across the eastern (transect A) and western (transect B) part of the gulf. The offset between the crustal thinning and the Gulf of Corinth is consistent with the hypothesis of a low-angle normal fault at 12 km depth below the western part of the Corinth rift and a ductile lower crust.

1993]. Anyway, the surface expression of the Corinth rift is offset from the imaged crustal thinning. Although at the eastern part of the rift the crustal thinning seems to be more or less at the vertical of the rift itself, the shift between the structures is maximum at the western part of the rift (Figure 7) and reaches some 20 km. This difference between the eastern and western parts of the Corinth rift could be consistent with the structural differences observed in fault geometry and with the differences in focal mechanisms. In the eastern part of the Corinth rift, fault plane solutions indicate about 45° dipping nodal planes, whereas in the western part, slip on low-angle planes ($\leq 30^\circ$) has been documented [Rietbrock *et al.*, 1996; Bernard *et al.*, 1997].

In the early 1980s, Wernicke [1985] first proposed a continental rifting model involving lithospheric low-angle normal faults known as the simple shear model, as opposed to the pure shear model of McKenzie [1978b]. Lister and Davis [1989] combined both models to propose an asymmetric rifting process accommodated by a crustal low-angle normal fault. Such rifting processes involve an asymmetry of the structures, which is obvious for the Gulf of Corinth (Figure 2), and an offset between the maximum crustal thinning and the maximum deformation inside the rift. For Corinth this offset increases as one goes westward because the direction of present rupture propagation is different from that of the Miocene crustal thinning. The rift might accommodate this offset by concentrating part of its deformation on a crustal low-angle normal fault, at ~ 12 km depth (Figure 7).

Previous seismological studies [Rietbrock *et al.*, 1996; Rigo *et al.*, 1996] suggested the existence of an active low-angle north dipping normal fault, 10-12 km beneath the western part of the Gulf of Corinth that could accommodate deformation in this region. This would be consistent with the model of Lister and Davis [1989]. Such a rift geometry could explain not only the offset of the structures but also the concentration of the deformation inside the gulf itself. Moreover, Pham *et al.* [1996] found a highly conductive layer between 10 and 15 km depth, probably corresponding to the location of a ductile zone, which seems consistent with a decoupling at this depth. This would favor a deformation model similar to that proposed by Lister and Davis [1989], which needs a crustal detachment horizon between the upper crust and upper mantle, located at the end of the low-angle normal fault.

6. Conclusions

Teleseismic travel time data provide a rather detailed image of the crust and upper mantle beneath the Corinth rift. The observed tomograms reveal that the velocity contrast is in the range of about -7% to $+8\%$ for this region. The main striking feature in the upper mantle is a NW-SE high-velocity body ($+5\%$) dipping northeastward and interpreted as the African subducting lithosphere. The shallow part of this slab is not resolved by the inversion because it is almost horizontal. Starting at ~ 70 km depth, the slab has a dip angle of $\sim 50^\circ$ - 60° with a quite regular shape (Plate 3). Al-

though the recorded seismicity seems to stop below 200 km depth, the slab should continue below this depth to explain the increase in amplitude in the deepest layers (up to +8% for ACH method), in agreement with previous studies [e.g., Spakman *et al.*, 1988; Piomallo and Morelli, 1997]. Synthetic tests using the observed ray distribution characteristics show low-velocity artefacts around the edges of the slab, similar to those observed in the inverted model. Vertical smearing does happen, although it does not cause the observed crustal anomalies.

In addition to imaging the African slab we also demonstrated that some important structures in the crust can be resolved. In particular, the major crustal anomalies are (1) a high-velocity body (+4%) located beneath the northern edge of the Gulf of Corinth and (2) a low-velocity anomaly located at the southwestern part of the array. The first anomaly may correspond to crustal thinning related to Miocene extension, which would have been created by necking instabilities, as first proposed by Armijo *et al.* [1996]. The second feature is related to crustal thickening at the SW, associated with the Hellenides structure. Both structures (crustal thinning and crustal thickening) could counterbalance the artefacts of the dipping slab in the crustal layers. The effect of a geological nappe cannot be ruled out. However, such a nappe has no surface expression, and it would have to correspond to a very strong velocity contrast in order to explain the observed anomaly.

Our results suggest that the present geometry of the Corinth rift comes from the superposition of two different events (Figure 7). Crustal thinning was first initiated by lithospheric boudinage at Miocene time and could have favored the initiation of rupture at the surface. Then the Corinth area would have been reactivated 1 Myr ago, possibly by the North Anatolian Fault propagation, as proposed by Armijo *et al.* [1996]. Changes in boundary conditions or preexisting heterogeneities could favor a westward rift propagation, different from the initial crustal thinning location. The resulting offset, with the maximum in the west, could now be accommodated by a low-angle north dipping normal fault at 10–12 km depth, delineating a possible detachment horizon. As the rupture propagates westward in the Corinth rift [Armijo *et al.*, 1996], the offset between the gulf itself and the crustal thinning will increase westward (Figure 7), and one can wonder how such an offset will be accommodated, even with a low-angle normal fault. Unfortunately, no relevant information is yet available in the extreme western part of the gulf. Crustal thinning may be ~5 km, although this cannot be determined accurately by teleseismic tomography, and extends over a width of 10–15 km. The proposed amount of crustal thinning was roughly calculated without taking into account the influence of the Hellenides structure that surely enhances the amplitude of the fast-velocity anomaly. Further studies on the crustal structure are currently being carried out, namely, receiver function and gravity modeling, in order to better constrain these structures.

No clear velocity anomaly can be related to the Evvia rift in this region. However, our study area is too limited regarding the Evvia structure, and a crustal thinning beneath Evvia or shifted away from it may have been missed or only

badly resolved with our array geometry. As it is difficult to deploy a wider array north of Evvia, other geophysical studies, independent of this one, should be done in order to bring additional constraints for this region.

Acknowledgments. We are grateful to Frédéric Masson for helpful discussion on the ACH method, and to Rolando Armijo, Alfred Hirn, and Laurent Jolivet for fruitful discussions. We want to thank Jérôme Ammann, Sébastien Chevrot, Véronique Farra, Emmanuel Gaucher, Georges Herquel, Thanassis Karamezinis, Sophie Le Rouzic, Kiriakas Pefitsetis and Éléonore Stutzmann for their help in the field. We are most grateful to the Associated Editors F. Tilmann and T. Taymaz for their helpful comments and review. This work was performed under EC Environment and Climate contract ENV4-CT96-0277 with additional financial support from INSU-IDYL program. This is IGP contribution 1666.

References

- Aki, K., A. Christofferson, and E. S. Husebye, Determination of the three-dimensional seismic structure of the lithosphere, *J. Geophys. Res.*, **82**, 277–296, 1977.
- Allemand, P., and J.-P. Brun, Width of continental rifts and rheological layering of the lithosphere, *Tectonophysics*, **188**, 63–69, 1991.
- Argus, D. R. G., C. D. Mets, and S. Stein, Closure of the Africa-Eurasia-North America plate motion circuit and tectonics of the Gloria fault, *J. Geophys. Res.*, **94**, 5585–5602, 1989.
- Armijo, R., B. Meyer, G. King, A. Rigo, and D. Papanastassiou, Quaternary evolution of the Corinth Rift and its applications for the late Cenozoic evolution of the Aegean, *Geophys. J. Int.*, **126**, 11–53, 1996.
- Bernard, P., et al., The $M_s=6.2$, June 15, 1995 Aigion earthquake (Greece): Evidence for low normal faulting in the Corinth rift, *J. Seismol.*, **1**, 131–150, 1997.
- Bijwaard, H., W. Spakman, and E. Engdahl, Closing the gap between regional and global travel time tomography, *J. Geophys. Res.*, **103**, 30,055–30,078, 1998.
- Bonneau, M., Évolution géodynamique de l'arc égéen depuis le Jurassique supérieur jusqu'au Miocène, *Bull. Soc. Géol. Fr.*, **24**, 229–242, 1982.
- Briole, P., A. Rigo, H. Lyon-Caen, J.-C. Ruegg, K. Papazissi, C. Mistakaki, A. Balodimou, G. Veis, D. Hatzfeld, and A. Deschamps, Active deformation of the Corinth Rift, Greece: Results from repeated GPS surveys between 1990 and 1995, *J. Geophys. Res.*, in press, 2000.
- Clarke, P., et al., Geodetic estimate of seismic hazard in the Gulf of Corinthos, *Geophys. Res. Lett.*, **24**, 1303–1306, 1997.
- Clarke, P., et al., Crustal strain in central Greece from repeated GPS measurements in the interval 1989–1997, *Geophys. J. Int.*, **135**, 195–214, 1998.
- Engdahl, R., R. van der Hilst, and R. Buland, Global teleseismic earthquake relocation with improved travel times and procedures for depth determination, *Bull. Seismol. Soc. Am.*, **88**, 722–743, 1998.
- Evans, J. R., and U. Achauer, Teleseismic velocity tomography using the ACH method: Theory and application to continental-scale studies, in *Seismic Tomography: Theory and Practice*, edited by H. Iyer and K. Hirahara, pp. 319–360, Chapman and Hall, New York, 1993.
- Evans, J., and J. Zucca, Active high-resolution tomography of compressional wave velocity and attenuation structure at Medicine Lake Volcano, northern California Cascade Range, *J. Geophys. Res.*, **93**, 15,016–15,036, 1988.
- Hatzfeld, D., On the shape of the subducting slab beneath the Peloponnese, Greece, *Geophys. Res. Lett.*, **21**, 173–176, 1994.
- Hatzfeld, D., and C. Martin, Intermediate depth seismicity in the Aegean defined by teleseismic data, *Earth Planet. Sci. Lett.*, **113**, 267–275, 1992.

- Hatzfeld, D., et al., The Hellenic subduction beneath the Peloponnese: First results of a microearthquake study, *Earth Planet. Sci. Lett.*, *93*, 283–291, 1989
- Jackson, J., J. Gagnepain, G. Houseman, G. King, P. Papadimitriou, C. Soufleris, and J. Virieux, Seismicity, normal faulting, and the geomorphological development of the Gulf of Corinth (Greece): The Corinth earthquakes of February and March 1981, *Earth Planet. Sci. Lett.*, *57*, 377–397, 1982.
- Jolivet, L., and M. Patriat, Ductile extension and the formation of the Aegean Sea, in *The Mediterranean Basins: Tertiary Extension Within the Alpine Orogen*, edited by B. Durand et al., *Geol. Soc. Spec. Publ.*, *156*, 427–456, 1999.
- Kahle, H.-G., V. Mueller, S. Mueller, and G. Veis, The Kephallonia transform fault and the rotation of the Apulian platform: Evidence from satellite geodesy, *Geophys. Res. Lett.*, *20*, 651–654, 1993.
- Kennett, B. L. N., and E. R. Engdahl, Traveltimes for global earthquake location and phase identification, *Geophys. J. Int.*, *105*, 429–465, 1991.
- Le Meur, H., J. Virieux, and P. Podvin, Seismic tomography of the Gulf of Corinth: A comparison of methods, *Ann. Geofis.*, *40*, 1–24, 1997.
- Le Pichon, X., and J. Angelier, The Hellenic arc and trench system. A key to the neotectonic evolution of the eastern Mediterranean area, *Tectonophysics*, *60*, 1–42, 1979.
- Le Pichon, X., N. Chamot-Rooke, and S. Lallemand, Geodetic determination of the kinematics of central Greece with respect to Europe: Implication for eastern Mediterranean tectonics, *J. Geophys. Res.*, *100*, 12,675–12,690, 1995.
- Lister, G., and G. Davis, The origin of metamorphic core complexes and detachment faults formed during Tertiary continental extension in the northern Colorado River region, U.S.A., *J. Struct. Geol.*, *11*, 65–94, 1989.
- Lundgren, P., D. Giardini, and R. M. Russo, A geodynamic framework for eastern Mediterranean kinematics, *Geophys. Res. Lett.*, *25*, 4007–4010, 1998
- Martinod, J., and P. Davy, Periodic instabilities during compression or extension of the lithosphere, I, Deformation modes from an analytical perturbation method, *J. Geophys. Res.*, *97*, 1999–2014, 1992.
- McClusky, S., et al., Global Positioning System constraints on plate kinematics and dynamics in the eastern Mediterranean and Caucasus., *J. Geophys. Res.*, *105*, 5695–5719, 2000.
- McKenzie, D., Active tectonics of the Alpine-Himalayan belt. The Aegean Sea and surroundings regions, *Geophys. J. R. Astron. Soc.*, *55*, 217–254, 1978a
- McKenzie, D., Some remarks on the development of sedimentary basins, *Earth Planet. Sci. Lett.*, *40*, 25–32, 1978b.
- Menke, W., *Geophysical Data Analysis. Discrete Inverse Theory*, Academic, San Diego, Calif., 1984.
- Mercier, J., Extensional-compressional tectonics associated with the Aegean Arc: Comparison with the Andean Cordillera of south Peru-north Bolivia, *Philos. Trans. R. Soc. London, Ser. A*, *300*, 337–355, 1981.
- Mouyiaris, N., et al., Seismotectonic map of Greece with seismological data, map, scale 1:500,000, *Inst. of Geol. and Miner. Explor.*, Athens, 1989.
- Noomen, R., T. Springer, B. Ambrosius, K. Herzberger, D. Kuijper, G. Mets, B. Overgaaauw, and K. Wakker, Crustal deformations in the Mediterranean area computed from SLR and GPS observations, *J. Geodyn.*, *21*, 73–96, 1996.
- Papazachos, B., V. Karakostas, C. Papazachos, and E. Scordilis, The geometry of the Wadati-Benioff zone and lithospheric kinematics in the Hellenic arc, *Tectonophysics*, *319*, 275–300, 2000.
- Papazachos, C., and G. Nolet, P and S deep velocity structure of the Hellenic area obtained by robust nonlinear inversion of travel times, *J. Geophys. Res.*, *102*, 8349–8367, 1997.
- Papazachos, C., P. Hatzidimitriou, D. Panagiotopoulos, and G. Tsokas, Tomography of the crust and upper mantle in south-east Europe, *J. Geophys. Res.*, *100*, 12,405–12,422, 1995.
- Pham, V. N., D. Boyer, G. Chouliaras, and P. Bernard, Conductivité électrique et structure de la croûte dans la région du Golfe de Corinthe (Grèce) d'après les résultats de sondage Magnéto-Tellurique (SMT), *C. R. Acad. Sci.*, *323*, 651–656, 1996.
- Piromallo, C., and A. Morelli, Imaging the Mediterranean upper mantle by p-wave travel time tomography, *Ann. Geofis.*, *40*, 963–979, 1997.
- Rietbrock, A., C. Tiberi, F. Scherbaum, and H. Lyon-Caen, Seismic slip on a low angle normal fault in the Gulf of Corinth: Evidence from high-resolution cluster analysis of microearthquakes, *Geophys. Res. Lett.*, *23*, 1817–1820, 1996.
- Rigo, A., H. Lyon-Caen, R. Armijo, A. Deschamps, D. Hatzfeld, K. Makropoulos, P. Papadimitriou, and I. Kassaras, A microseismic study in the western part of the Gulf of Corinth (Greece). Implications for large-scale normal faulting mechanisms, *Geophys. J. Int.*, *126*, 663–688, 1996.
- Roberts, S., and J. Jackson, Active normal faulting in central Greece. An overview, in *The Geometry of Normal Faults*, edited by A.M. Roberts, G. Yieldings, and B. Freeman, *Geol. Soc. Spec. Publ.*, *56*, 125–142, 1991.
- Spakman, W., M. Wortel, and N. Vlaar, The Hellenic subduction zone: A tomographic image and its geodynamics implications, *Geophys. Res. Lett.*, *15*, 60–63, 1988.
- Steck, L., and W. Prothero, A 3-D raytracer for teleseismic body-wave arrival times, *Bull. Seismol. Soc. Am.*, *81*, 1332–1339, 1991.
- Taymaz, T., J. Jackson, and R. Westaway, Earthquake mechanisms in the Hellenic Trench near Crete, *Geophys. J. Int.*, *102*, 695–731, 1990.
- Taymaz, T., J. Jackson, and D. McKenzie, Active tectonics of the north and central Aegean Sea, *Geophys. J. Int.*, *106*, 433–490, 1991.
- Thurber, C., Earthquake locations and three-dimensional crustal structure in the Coyote Lake Area, central California, *J. Geophys. Res.*, *88*, 8226–8236, 1983.
- Van Decar, J. C., and R. S. Crosson, Determination of teleseismic relative phase arrival times using multi-channel cross-correlation and least squares, *Bull. Seismol. Soc. Am.*, *80*, 150–169, 1990
- van der Hilst, R., and R. Snieder, High-frequency precursors to P wave arrivals in New Zealand: Implications for slab structure, *J. Geophys. Res.*, *101*, 8473–8488, 1996
- Weiland, C., L. Steck, P. Dawson, and V. Korneev, Nonlinear teleseismic tomography at Long Valley caldera, using three-dimensional minimum travel time ray tracing, *J. Geophys. Res.*, *100*, 20,379–20,390, 1995
- Wernicke, B., Uniform-sense normal simple shear of continental lithosphere, *Can. J. Earth Sci.*, *22*, 108–125, 1985

U. Achauer and C. Tiberi, Laboratoire de Sismologie, EOST, 5 rue René Descartes, F-67084 Strasbourg Cedex, France. (Ulrich.Achauer@eost.u-strasbg.fr; Christel.Tiberi@eost.u-strasbg.fr)

D. Hatzfeld, LGIT, Domaine Universitaire, 1381 rue de la piscine, BP 53, 38041 Grenoble Cedex 09, France. (Denis.Hatzfeld@obs.ujf-grenoble.fr)

E. Karagianni, A. Kiratzi, E. Louvari, and D. Panagiotopoulos, Department of Geophysics, University of Thessaloniki, Thessaloniki, Greece (karagian@geo.auth.gr; kiratzi@geo.auth.gr; louvari@geo.auth.gr; panagiot@geo.auth.gr)

I. Kassaras, G. Kaviris, M. Makropoulos and P. Papadimitriou, Department of Geophysics and Geothermy, University of Athens, Athens, Greece.

H. Lyon-Caen, Laboratoire de Géologie, ENS, 24 rue Lhomond, 75005 Paris, France. (Helene.Lyon.Caen@ens.fr)

(Received November 9, 1999, revised May 3, 2000, accepted June 12, 2000)